European Radiology (2021) 31:8388–8398
https://doi.org/10.1007/s00330-021-07966-y

MAGNETIC RESONANCE

Evaluation of amide proton transfer-weighted imaging for endometrial carcinoma histological features: a comparative study with diffusion kurtosis imaging

Nan Meng[1,2] · Xuejia Wang[3] · Jing Sun[4] · Zhun Huang[5] · Zhen Yang[4] · Jie Shang[6] · Yan Bai[1,2] · Wei Wei[1,2] · Dongming Han[3] · Hui Han[7] · Kaiyu Wang[8] · Fengmin Shao[9] · Meiyun Wang[1,2]

Received: 8 January 2021 / Revised: 4 March 2021 / Accepted: 31 March 2021 / Published online: 21 April 2021

Abstract

Objectives To investigate whether amide proton transfer-weighted imaging (APTWI) and diffusion kurtosis imaging (DKI) can be used to evaluate endometrial carcinoma (EC) in terms of clinical type, histological grade, subtype, and Ki-67 index.

Methods Eighty-eight patients with EC underwent pelvic DKI and APTWI. The non-Gaussian diffusion coefficient (D_{app}), apparent kurtosis coefficient (K_{app}), and magnetization transfer ratio asymmetry (MTRasym (3.5 ppm)) were calculated and compared based on the clinical type (type I, II), histological grade (high- and low-grade), and subtype (endometrioid adenocarcinoma (EA) and non-EA). Correlation coefficients were calculated for each parameter with histological grades and the Ki-67 index.

Results The MTRasym (3.5 ppm) and K_{app} values were higher in the type II group and high-grade group than in the type I and low-grade groups, respectively, while the D_{app} values were lower in the type I and low-grade groups, respectively (all $p < 0.05$). The K_{app} value was higher in the EA group than in the non-EA group ($p = 0.022$). The K_{app} value was the only independent predictor for the histological grade of EA and the clinical type of EC. The AUC (DKI) was higher than the AUC (APTWI) in the identification of type I and II EC and high- and low-grade EA ($Z = 2.042, 2.013$, $p = 0.041, 0.044$), while in the identification of EA and non-EA, only the difference in K_{app} was statistically significant. Moreover, the K_{app} and MTRasym (3.5 ppm) values and D_{app} values correlated positively and negatively, respectively, with histological grade ($r = 0.759, 0.555, 0.624$, and 0.462, all $p < 0.05$) and Ki-67 index ($r = -0.704, -0.507$, all $p < 0.05$).

Conclusion Both DKI- and APTWI-related parameters have potential as imaging markers in estimating the histological features of EC, while DKI shows better performance than APTWI in this study.

Nan Meng and Xuejia Wang contributed equally to this work and should be considered co-first authors.

✉ Fengmin Shao
fengminshao@126.com

✉ Meiyun Wang
mywang@ha.edu.cn

[1] Department of Medical Imaging, Zhengzhou University People's Hospital & Henan Provincial People's Hospital, Zhengzhou, Henan, China

[2] Academy of Medical Sciences, Zhengzhou University, Zhengzhou, Henan, China

[3] Department of MR, The First Affiliated Hospital, Xinxiang Medical University, Weihui, China

[4] Department of Pediatrics, Zhengzhou Central Hospital, Zhengzhou University, Zhengzhou, China

[5] Department of Medical Imaging, Henan University People's Hospital & Henan Provincial People's Hospital, Zhengzhou, Henan, China

[6] Department of Pathology, The First Affiliated Hospital, Xinxiang Medical University, Weihui, China

[7] Biomedical Imaging Research Institute, Cedars-Sinai Medical Center, Los Angeles, CA, USA

[8] MR Research China, GE Healthcare, Beijing, China

[9] Department of Nephrology, Zhengzhou University People's Hospital & Henan Provincial People's Hospital, Zhengzhou, Henan, China

Key Points

- *DKI and APTWI can be used to preliminarily evaluate the histological characteristics of endometrial carcinoma (EC).*
- *The K_{app} was the only independent predictor for the histological grade of EA and the clinical type of EC.*
- *The K_{app}, MTRasym (3.5 ppm), and D_{app} correlated positively and negatively, respectively, with histological grade and Ki-67 index.*

Keywords Diffusion magnetic resonance imaging · Magnetization transfer contrast imaging · Endometrial neoplasms

Abbreviations

APTWI	Amide proton transfer-weighted imaging
D_{app}	Non-Gaussian diffusion coefficient
DKI	Diffusion-kurtosis imaging
EA	Endometrioid adenocarcinoma
EC	Endometrial carcinoma
FIGO	International Federation of Gynecology and Obstetrics
K_{app}	Apparent kurtosis coefficient
MTRasym (3.5 ppm)	Magnetization transfer ratio asymmetry at 3.5 ppm
SI	Signal intensity

Introduction

Endometrial carcinoma (EC) is a common malignant tumor of the female reproductive system, with high morbidity and mortality worldwide [1, 2]. Studies to date have shown that clinical type, histological grade, subtype, and the Ki-67 index can all have important effects on the treatment and prognosis of EC patients. For example, Bokhman et al [3] showed that type I (estrogen-dependent) EC was more sensitive to hormone therapy and had a better prognosis than type II (nonestrogen-dependent) EC. Furthermore, Scholten et al [4] found that the 5-year survival rate of patients with low-grade (grades 1, 2) EC was significantly higher than that of patients with high-grade (grade 3) EC (92%, 94% vs 63%). The study of Kitson et al [5] also reported that the level of the Ki-67 index can serve as an effective biological marker for EC disease assessment.

In clinical practice, preoperative biopsy is widely used in the evaluation of EC histological features. However, due to the influence of multiple factors, such as operator experience, tumor heterogeneity, and lesion size, this method may not be sufficient to make correct diagnoses for the clinical types, histological grades or subtypes, and Ki-67 index [6, 7]. Magnetic resonance imaging (MRI) is currently recognized as a reliable means of noninvasive detection and evaluation of EC [8, 9]. However, conventional MRI sequences based on morphological imaging often cannot well reflect the microscopic information of lesions, which makes it difficult to provide more detailed guidance for relevant clinical diagnosis and treatment programs [10, 11]. Furthermore, the advent of diffusion-weighted imaging (DWI) and dynamic contrast-enhanced imaging (DCE-MRI) has greatly improved the reliability of MRI in predicting aspects of EC lesions [12, 13]. Nonetheless, in the absence of biopsy, there are still great challenges in the assessment of micropathological features such as clinical type, histological grade, subtype, and Ki-67 index in EC patients using conventional MRI alone. Diffusion kurtosis imaging (DKI) is a type of diffusion imaging technology that utilizes the motion of water molecules in tissue as a non-Gaussian distribution [14]. Compared with DWI, DKI more accurately describes the diffusion characteristics of water molecules in tissue; thus, it has higher sensitivity with regard to reflecting the complexity of the microstructure of tissue [15]. Due to this advantage, DKI has been widely used in glioma grading [16], stroke assessment [17], and diagnosis and prognosis evaluation of breast [18] and cervical [19] cancer as well as in other fields. Amide transfer-weighted imaging (APTWI) is an MRI molecular imaging technology proposed by Zhou et al [20] that is based on the chemical exchange between amide protons and water protons and can achieve noninvasive quantitative assessment of mobile protein and polypeptide concentrations in tissues without the use of contrast agents. Previous studies have confirmed that APTWI can be implemented for the diagnosis, identification, and prognosis assessment of some diseases [19, 21, 22]. However, in terms of EC research, only a few small sample studies thus far have separately reported that APTWI [23]- and DKI [24]-related parameters can be preliminarily used as imaging markers for the noninvasive assessment of EC histological grade.

This study aimed to investigate APTWI and DKI in the evaluation of EC in terms of clinical type, histological grade, subtype, and Ki-67 index, with the goal of providing new help for the diagnosis and treatment of EC patients.

Materials and methods

Study population

The Ethics Committee of the local institution approved this prospective study. Written informed consent was acquired from each patient before scanning. From August 2017 to

Table 1 Clinicopathologic characteristics of the patients

Characteristics	Type I (n = 68)	Type II (n = 20)
Age (years)	57.38 ± 7.46 (41–70)	62.95 ± 9.04 (40–71)
Maximum diameter (mm)	51.50 ± 13.68 (22–81)	56.40 ± 14.36 (33–100)
Histological type n (%)		
Endometrioid	68 (100.00%)	13 (65.00%)
Serous	0 (0.00%)	4 (20.00%)
Clear-cell	0 (0.00%)	3 (15.00%)
Histological grade n (%)		
Grade 1	45 (66.18%)	0 (0.00%)
Grade 2	23 (33.82%)	0 (0.00%)
Grade 3	0 (0.00%)	20 (100.00%)
FIGO stage n (%)		
IA	32 (47.06%)	4 (20.00%)
IB	16 (23.53%)	3 (15.00%)
II	5 (7.35%)	3 (15.00%)
IIIA	3 (4.41%)	2 (10.00%)
IIIB	3 (4.41%)	2 (10.00%)
IIIC1	2 (2.94%)	1 (5.00%)
IVA	3 (4.41%)	2 (10.00%)
IVB	4 (5.88%)	3 (15.00%)
Ki-67 index n (%)		
≤ 10% (−)	3 (4.41%)	0 (0.00%)
11%–25% (+)	19 (27.94%)	0 (0.00%)
26%–50% (+ +)	22 (32.35%)	6 (30.00%)
≥ 51% (+ + +)	24 (35.29%)	14 (70.00%)

April 2020, a consecutive series of 130 female patients were enrolled for MRI in this study due to suspicion of having EC by computed tomography (CT) or ultrasound (US). The exclusion criteria were as follows: (1) pathologic findings were non-EC (n = 9); (2) patients who were unable to complete all imaging sequences due to claustrophobia or the long scanning time (n = 6); (3) the quality of APTWI or DKI images was hampered by motion or ghosting artifacts (n = 8); (4) the maximum area of EC was less than 50 pixels (392 mm^2) on the axial plane of APTWI or DKI given the effect of image noise (n = 7); (5) chemotherapy, radiotherapy, or surgery was performed before scanning (n = 9); and (6) unclear pathological or immunohistochemistry results (n = 3). Ultimately, 88 patients were included in the study (age range, 41–73 years; mean age, 58 years) (Fig. 1, Table 1).

Image acquisition

MR imaging was performed with a 3.0-T MR scanner (Discovery MR750, GE Healthcare) equipped with a 16-channel phased-array body coil. For all sequences, patients were placed in the supine position feet-first into the scanner and with a partially full bladder. Before the examination, 40 mg of hyoscine butyl bromide (Buscopan; Boehringer) was administered intramuscularly to reduce bowel motion. First, two-dimensional axial T1-weighted imaging (T1WI), T2-weighted imaging (T2WI), and DWI [11] scans were performed. Next, with reference to T1WI, T2WI, and DWI images, a radiologist with 10 years of experience selected slices on which a tumor appeared to be present as the scan sections for APTWI and DKI. A total of 5 b-values (0, 500, 1000, 1500, and 2000 s/mm^2), with 30 diffusion directions, were used in DKI [14, 15, 24]. APTWI was performed by using a saturation power level of 2.0 μT and a saturation pulse (T_{sat}) with a duration of 0.5 s [21, 23–25]. A total of 52 frequencies, including 49 offsets ranging from −600 to + 600 Hz with an interval of 25 Hz and a frequency 5000 Hz (3 times) far from the resonant frequency, were used for the APTWI and z-spectrum scans for signal normalization. The water saturation shift reference (WASSR) was applied for B_0 correction.

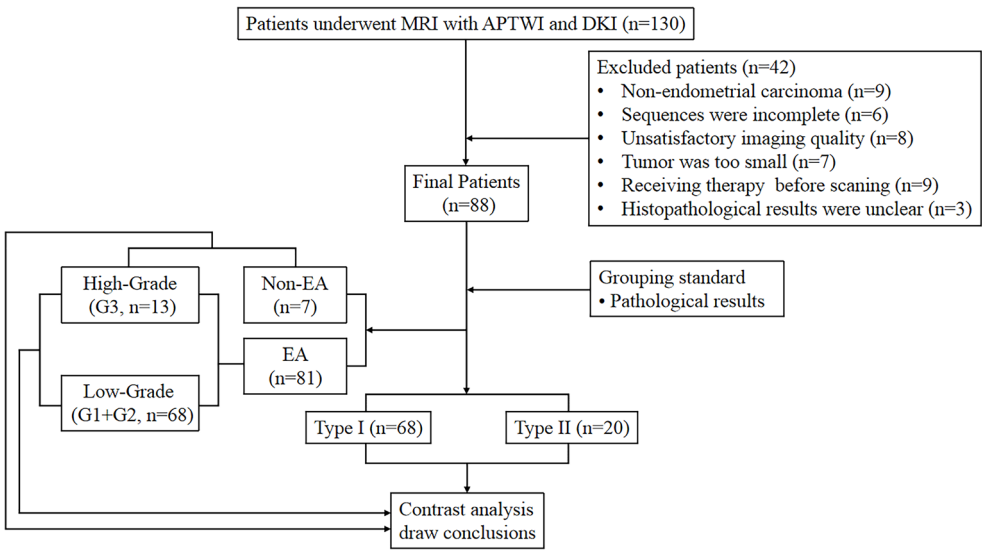

Fig. 1 Flow diagram of the patient selection process

Finally, a DCE-MRI scan was performed in which a volume of gadopentate dimeglumine (Gd-DTPA, Bayer Pharmaceutical) was intravenously injected (0.1 mL/kg, 2.0 mL/s) using an automatic injector. The details of each protocol are shown in Table 2.

Data postprocessing

All MR images were independently analyzed by 2 radiologists (with 6 and 8 years of experience, respectively) who were blinded to each other's results as well as the clinical data and pathology reports. The DKI and APTWI images were analyzed using a postprocessing workstation (Advantage Workstation 4.6, GE Healthcare) equipped with special software (GE FuncTool). For K_{app}, D_{app}, and MTRasym (3.5 ppm) maps, regions of interest (ROIs), excluding areas with necrotic regions, obvious signals or artifacts from a hemorrhage, cystic degeneration, and blood vessels, were drawn along the tumor edge at every cross-section of the tumor tissue using T1WI, T2WI, DWI, and DCE-MRI as references. The final value of each lesion parameter was the average value of the corresponding parameter on all slices.

DKI parameters were calculated using the following equation:

$$S_b = S_0 \times \exp\left(-b \times D_{app} + b^2 \times {D_{app}}^2 \times K_{app}/6\right)$$

where S_0 and S_b represent the signal intensity (SI) under different b-values (0 s/mm^2 or other values), respectively; K_{app} (arbitrary units) indicates kurtosis and represents the degree of deviation from the Gaussian distribution; and D_{app} ($\times 10^{-3}$ mm^2/s) indicates diffusivity and represents the diffusion coefficient corrected for non-Gaussian bias [14, 15].

APTWI parameters were calculated using the equation:

$$\text{MTRasym (3.5 ppm)} = [S_{sat}\ (-3.5\ \text{ppm}) - S_{sat}\ (+3.5\ \text{ppm})]/S_0$$

where S_{sat} and S_0 are the SIs obtained with and without selective saturation, respectively; the magnetization transfer ratio was defined as $1 - S_{sat}/S_0$, and MTRasym (3.5 ppm) represents the magnetization transfer ratio asymmetry at 3.5 ppm downfield from the water signal [20, 21].

Histopathologic analysis

A pathologist (with 8 years of experience), who was blinded to the MRI data, analyzed all surgically resected specimens of each patient. The clinical type, histological grade, and subtype were determined by hematoxylin/eosin (HE) staining. A murine Ki-67 monoclonal antibody (M3G4, Celnovte) was used to determine the Ki-67 index. Referring to the International Federation of Gynecology and Obstetrics (FIGO) grading system [26] and previous studies [3, 27], the specimens were classified into the following groups: type I (grade 1 and grade 2 endometrioid adenocarcinoma (EA)) and type II (grade 3 EA and non-EA (clear cell and serous carcinoma)) EC groups, EA (grade 3) and non-EA groups, and low-grade (grade 1 and grade 2) and high-grade (grade 3) EA groups.

Statistical analysis

The software MedCalc (Version 15.0; MedCalc Software) and SPSS (Version 23.0; IBM) were employed for statistical analyses. Interobserver reliability is described with the intraclass correlation coefficient (ICC) ($r \geq 0.75$, excellent agreement;

Table 2 Imaging protocol parameters

Parameters	T1WI	T2WI	DWI	DKI	APTWI	DCE-MRI
Sequence	2D-FSE	2D-FSE	2D-SS-EPI	2D-SS-EPI	2D-EPI	3D-LAVA
Orientation	Axial	Axial	Axial	Axial	Axial	Axial
TR/TE (ms)	605/8	5455/109	6000/60.5	2500/58.9	3000/12	4.2/2.1
FOV (cm^2)	36 × 36	36 × 36	36 × 36	36 × 36	36 × 36	36 × 36
Matrix	320 × 224	320 × 224	128 × 128	128 × 128	128 × 128	320 × 320
Bandwidth (Hz/pixel)	62.50	83.33	250	250	250	83.33
Slice thickness	5	5	5	5	5	1
No. of sections	20	20	20	5-15	1	80
NEX	1	1	1, 4	2	1	0.7
Fat suppression	/	STIR	STIR	SPECIAL	STIR	FLEX
b-values (s/mm^2)	/	/	0, 1000	0, 500, 1000, 1500, 2000	/	/
Respiratory compensation	Free	Free	Free	Free	Free	Breath holding
Scan time	1 min 57 s	1 min 33 s	1 min 24 s	5 min 28 s	2 min 36 s	0:09 (each phase)

FSE fast spin echo, *SS-EPI* single shot echo planar imaging, *TR/TE* repetition time/echo time, *FOV* field of view, *NEX* number of excitations, *LAVA* liver acquisiton with volume assessment, *FLEX* flexible, *STIR* short-inversion time (TI) recovery, *SPECIAL* spectral inversion at lipids

$0.60 \leq r < 0.75$, good agreement; $0.40 \leq r < 0.60$, fair agreement; and $r < 0.40$, poor agreement) [23]. The Shapiro-Wilk test was applied to evaluate whether the data of each group followed a normal distribution. The comparison of each parameter between different groups was analyzed with the independent sample *t* test. Receiver operating characteristic (ROC) curves were generated, and the Delong test was performed to determine which parameter was suitable for the evaluation of EC histological features. Logistic regression analyses were used to identify independent factors and combination diagnosis. The Spearman rank and Pearson correlation were employed to describe the correlation of each parameter with histologic grade and Ki-67 index, respectively. A correlation coefficient (*r*) of 0.75–1.00 was considered to indicate a good correlation, 0.50–0.74 a moderate correlation, 0.25–0.49 a mild correlation, and 0.24 or lower little or no correlation. Results with $p < 0.05$ were considered to be statistically significant [18].

Results

Characteristics of the patients

Table 1 shows the clinicopathological characteristics of all patients.

Consistency test

The ICCs between the two readers were as follows: K_{app}, 0.861; D_{app}, 0.843; and MTRasym (3.5 ppm), 0.757. Therefore, the two readers' averaged values of the parameter were used for the final analysis.

Differences in parameters

The D_{app} value was higher, and the K_{app} and MTRasym (3.5 ppm) values were lower in the type I group than in the type II group ($p = 0.002$, < 0.001, and < 0.001). Although the K_{app} value was higher in the EA group than in the non-EA group ($p = 0.022$), the difference in D_{app} and MTRasym (3.5 ppm) values between the two groups was not significant ($p > 0.05$). Additionally, the D_{app} value was higher, and the K_{app} and MTRasym (3.5 ppm) values were lower in the low-grade group than in the high-grade group ($p = 0.002$, < 0.001, and $= 0.001$) (Figs. 2 and 3, Table 3).

Regression analyses

Age, tumor size, FIGO stage, and related parameters were all included in the analysis. Univariate analysis revealed that FIGO stage, K_{app}, D_{app}, and MTRasym (3.5 ppm) were independent predictors for the histological grade of EA, and age, FIGO stage, K_{app}, D_{app}, and MTRasym (3.5 ppm) were independent predictors for the clinical type of EC. Multivariable analysis revealed that K_{app} was the only independent predictor for the histological grade of EA and the clinical type of EC ($p = 0.004$ and 0.02, respectively) (Table 4).

Diagnostic performance of different parameters

Regarding the identification of type I and type II EC, AUC (K_{app}) > AUC (D_{app}) > AUC (MTRasym (3.5 ppm)) was higher, but the difference between the AUCs of each parameter was not significant ($p > 0.05$). According to the different imaging methods, the AUC (DKI) was nearly significantly higher than AUC (APTWI) ($Z = 2.042$, $p = 0.041$), where AUC (DKI) means AUC (K_{app}+ D_{app}), AUC (APTWI) means AUC (MTRasym (3.5 ppm)). Regarding the identification of EA and non-EA, only the AUC of the K_{app} value was significant (AUC = 0.846, $p = 0.003$). Based on a comparison of high- versus low-grade EA, AUC (K_{app}) > AUC (D_{app}) > AUC (MTRasym (3.5 ppm)) and the difference in AUC between K_{app} and MTRasym (3.5 ppm) values were significant ($Z = 2.031$, $p = 0.042$). According to the different imaging methods, the AUC (DKI) was nearly significantly higher than the AUC (APTWI) ($Z = 2.013$, $p = 0.044$) (Fig. 4, Table 5).

Correlation analysis

K_{app} showed good and moderate positive correlations with histological grade and the Ki-67 index, respectively ($r = 0.759$, 0.624, $p < 0.05$). D_{app} was moderately and negatively correlated with histological grade and the Ki-67 index ($r = -0.704$, -0.507, $p < 0.05$). MTRasym (3.5 ppm) showed a moderate and mild positive correlation with histological grade and the Ki-67 index, respectively ($r = 0.555$, 0.462, $p < 0.05$) (Fig. 5).

Discussion

Evaluation of APTWI for EC

Our analyses revealed that APTWI aids in the discrimination of EC of different clinical types and histological grades. The function of APTWI to reflect lesion characteristics is accomplished via the detection of the mobile protein and polypeptide contents of lesions [20, 21]. Previous studies have shown that the MTRasym (3.5 ppm) value is mainly related to the following factors: high cellularity, nuclear atypia, microscopic necrosis, and microvessel density (MVD) [24, 28, 29]. In this study, the type I and low-grade groups included highly differentiated and moderately differentiated lesions, but the type II and high-grade groups included poorly differentiated lesions. In terms of EC, the pathologic features of poorly differentiated

Table 3 Comparison of different parameters among different groups

Groups	Age (year)	K_{app}	D_{app} ($\times 10^{-3}$ mm^2/s)	MTRasym (3.5 ppm) (%)
Histologic type				
Type I (n = 68)	57.38 ± 7.46	0.82 ± 0.07	1.14 ± 0.12	3.23 ± 0.55
Type II (n = 20)	62.95 ± 9.04	0.89 ± 0.04	1.02 ± 0.09	3.65 ± 0.39
t-value	−2.514	−5.119	4.469	−3.246
p value	0.018	< 0.001	< 0.001	0.002
Histological subtype				
EA (n = 13)	60.92 ± 9.94	0.92 ± 0.04	1.02 ± 0.10	3.66 ± 0.41
Non-EA (n = 7)	66.71 ± 5.99	0.87 ± 0.04	1.03 ± 0.09	3.64 ± 0.39
t-value	−1.623	2.632	−0.157	0.09
p value	0.122	0.022	0.877	0.928
Histologic grades				
Low (n = 68)	57.38 ± 7.46	0.82 ± 0.07	1.14 ± 0.12	3.23 ± 0.55
High (n = 13)	59.38 ± 11.66	0.92 ± 0.04	1.02 ± 0.10	3.69 ± 0.41
t-value	−0.803	−5.087	3.769	−3.551
p value	0.424	< 0.001	0.001	0.002

EA grade 3 endometrioid adenocarcinoma, *Non-EA* clear cell and serous carcinoma, *High-grade* G1+G2, *Low-grade* G3

carcinoma include a tighter tissue structure, greater nuclear atypia, and more microscopic necrosis than highly and moderately differentiated carcinoma [13, 30]. In addition, recent studies have shown that type II EC is associated with higher serum levels of vascular endothelial growth factor (VEGF) [31] and that many enhancement parameters are also higher in type II than in type I carcinomas [32]. Due to these features, the mobile protein and polypeptide contents of the type II and high-grade groups are greater than those of the type I and low-grade groups, resulting in higher MTRasym (3.5 ppm) values. Additionally, this study found no significant difference in the MTRasym (3.5 ppm) values between the EA and non-EA groups. The explanation for this result may be related to their similar degree of differentiation. Ki-67 is a nuclear nonhistone protein in proliferative-phase cells. In general, the higher its expression level is, the greater the density of EC cells, the lower the differentiation, and the greater the invasiveness [5]. Therefore, we think that the increase in the MTRasym (3.5 ppm) value in the high Ki-67 index lesions is related to high cellularity and nuclear atypia, among other features.

An important issue with APTWI is the choice of T_{sat}. A long T_{sat} was beneficial to obtain good contrast but also increased the probability of motion artifacts, especially during pelvic MRI. Most previous publications have suggested that APTWI with a T_{sat} of approximately 0.5 s was sufficient to evaluate pelvic lesions (such as EA, prostate cancer, and cervical cancer) [23, 25, 33]. Therefore, we applied a T_{sat} of 0.5 s in this study. However, it is necessary to further study the duration of the saturation radio frequencies.

In this study, we used echo planar imaging (EPI) acquisition for APTWI. Generally, turbo spin echo (TSE)–based APTWI [34] is less sensitive to susceptibility effect and superior in signal-noise ratio (SNR) than EPI-based APTWI. However, EPI is faster in acquisition, and when the image quality is acceptable, under the same time, using EPI acquisition could obtain more saturation spectra with different frequency offsets to improve quantitative accuracy. At present, TSE-based APTWI combined with acceleration schemes has been developed [34, 35], which is promising for clinical usage.

Evaluation of DKI for EC

Our analyses revealed that compared with the type II and high-grade groups, the diffusion of water molecules in the type I and low-grade groups is less restricted, and the degree of deviation from a Gaussian distribution is lower. According to previous studies, differences in tissue differentiation levels may be an important reason for the above results [16, 24]. Compared with the moderately and highly differentiated type I and low-grade groups, the poorly differentiated type II and high-grade groups tended to have a tighter tissue structure and more significant tissue heterogeneity. The former limits the diffusion velocity of water molecules; as the latter increases the deviation of the diffusion motion of water molecules, its D_{app} value decreases, and the K_{app} value increases. In addition, we also found that only the K_{app} value could distinguish the EA group and the non-EA group. The possible reasons are as follows: (1) Both the EA and non-EA groups are poorly differentiated tumors, and they to some extent are similar in features of cell proliferation and nuclear atypia. Therefore, it is difficult to use the D value, which is mainly affected by the above factors, to distinguish differences between them. (2) EA is mainly characterized by high dysplasia of glandular cells,

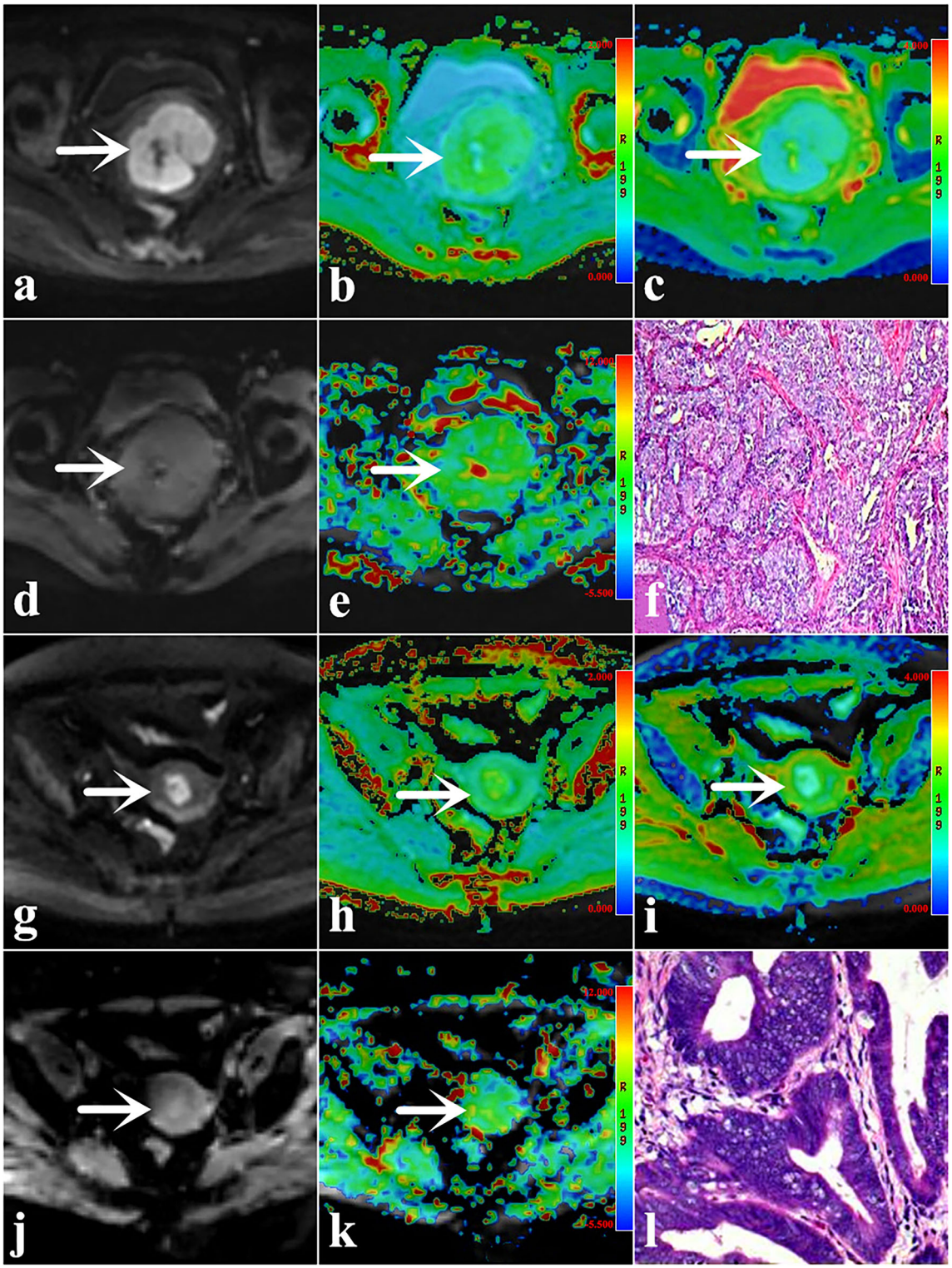

Fig. 2 **a**–**f** Images in a 58-year-old woman with type II, high-grade (grade 3) EA (arrowheads, Ki-67 = 60%). Averaged parameters values obtained by 2 readers were as follows: K_{app} = 0.946, D_{app} = 0.913×10^{-3} mm^2/s, MTRasym (3.5 ppm) = 3.78%. **g**–**l** Images in a 49-year-old woman with type I, low-grade (grade 1) EA (arrowheads, Ki-67 = 30%). Averaged parameters values obtained by 2 readers were as follows: K_{app} = 0.787, D_{app} = 1.227×10^{-3} mm^2/s, MTRasym (3.5 ppm) = 2.74%. **a**, **g** DWI original maps (b = 1000 s/mm^2), **b**, **h** pseudo colored maps of K_{app}, **c**, **i** pseudo colored maps of D_{app}, **d**, **j** APTWI original maps, **e**, **k** pseudo colored maps of MTRasym (3.5 ppm), **e**, **f** pathological images (original magnification, × 100)

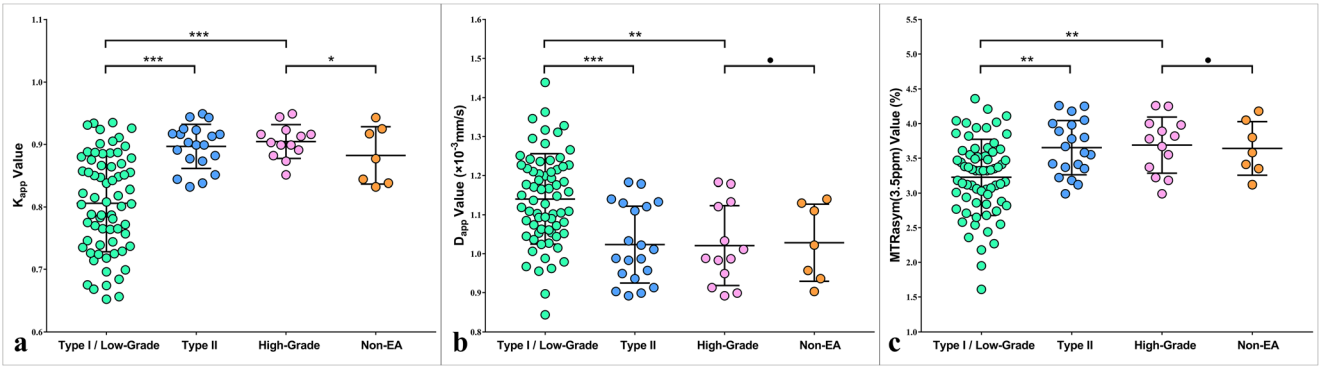

Fig. 3 Plots show individual data points, averages, and standard deviations of K_{app} (**a**), D_{app} (**b**), and MTRasym (3.5 ppm) (**c**) in different groups. Individual points are averages of values calculated by 2 readers. *$p < 0.05$, **$p < 0.01$, ***$p < 0.001$, and •$p > 0.005$

whereas serous carcinoma and clear-cell carcinoma display dense papillary and solid lamellar growth, respectively [36]. The difference in cell type and growth mode might be the reason for the difference in K_{app} values between the EA and non-EA groups. This study also indicated that DKI-related parameters can be applied as potential imaging markers to evaluate cell proliferation in EC. The reason may be as follows: in lesions with a high Ki-67 index, the cell proliferation ability was strong, and the tissue structure was compact [37]; therefore, the diffusion movement of water molecules was significantly restricted, and the D_{app} value was reduced. Additionally, a high Ki-67 index indicates a high degree of cell malignancy, high nuclear atypia, and more tissue necrosis. All these factors increase the heterogeneity of pathological tissues to different degrees and then cause a rise in the K_{app} value.

The DKI-related parameters were best estimated using 5–7 *b*-values in the range of 300–2000 s/mm^2 [14–18]. The reasons were as follows: the maximum *b*-value of 2000 s/mm^2 can obtain a sufficient signal-to-noise ratio while effectively reducing the apparent departure of diffusion kurtosis from linearity, and the minimal *b*-value of 300 s/mm^2 can reduce the influence of perfusion on the diffusion metrics. The *b*-values (0, 500, 1000, 1500, and 2000 s/mm^2) of this study were basically consistent with the above conclusion. Therefore, the reliability of the related parameters is relatively high.

Comparison of DKI and APTWI

In this study, the AUC (DKI) was nearly significantly higher than the AUC (APTWI) in the identification of type I and II

Table 4 Univariate and multivariate analyses for identifying high- and low-grade EA

Parameters	Univariate analyses		Multivariable analyses	
	OR (95% CI)	*p* value	OR (95% CI)	*p* value
High- and Low-grade EA				
Age (year)	1.287* (0.697–2.387)	0.420	/	/
Tumor size (mm)	1.097* (0.605–1.990)	0.761	/	/
FIGO stage	1.268 (1.003–1.604)	**0.048**	0.967 (0.702–1.331)	0.836
K_{app}	12.436* (3.081–50.200)	**< 0.001**	9.619* (2.062–44.871)	**0.004**
D_{app} (×10^{-3} mm^2/s)	0.301* (0.137–0.659)	**0.003**	0.629* (0.221–1.791)	0.385
MTRasym (3.5 ppm) (%)	3.018* (1.338–6.806)	**0.008**	1.250* (0.444–3.518)	0.673
Type I and type II EC				
Age (year)	1.817* (1.039–3.177)	**0.036**	1.579* (0.848–2.940)	0.150
Tumor size (mm)	1.421* (0.860–2.347)	0.170	/	/
FIGO stage	1.229 (1.059–1.595)	**0.012**	1.133* (0.599–2.140)	0.702
K_{app}	5.975* (2.439–14.639)	**< 0.001**	3.435* (1.216–9.703)	**0.020**
D_{app} (×10^{-3} mm^2/s)	0.303* (0.155–0.594)	**0.001**	0.555* (0.233–1.324)	0.184
MTRasym (3.5 ppm) (%)	2.919* (1.470–5.795)	**0.002**	1.636* (0.689–3.880)	0.264

All factors with $p < 0.1$ in univariate analyses were included in multivariate regression analyses. *OR* odds ratio, *CI* confidence interval. *OR for per 1 standard deviation. The bold typeface in the table indicates the logistic regression analyses with statistical significance

Table 5 Analysis of the diagnostic performance for K_{app}, D_{app}, and MTRasym (3.5 ppm) in discriminating different group

Parameters	AUC (95% CI)	*p* value	Cutoff	Sensitivity	Specificity
Type I vs type II					
K_{app}	0.837 (0.743–0.907)	< 0.001	0.845	95.00% (83/88)	64.71% (57/88)
D_{app} ($\times 10^{-3}$ mm^2/s)	0.774 (0.672–0.856)	< 0.001	1.033	65.00% (57/88)	83.82% (74/88)
APTWI [MTRasym (3.5 ppm) (%)]	0.732 (0.627–0.821)	< 0.001	3.340	80.00% (70/88)	55.88% (49/88)
DKI (K_{app}+D_{app})	0.870 (0.781–0.932)	< 0.001	/	/	/
EA vs non-EA					
K_{app}	0.846 (0.617–0.966)	0.003	0.847	92.31% (18/20)	85.71% (17/20)
D_{app} ($\times 10^{-3}$ mm^2/s)	0.516 (0.286–0.742)	0.907	/	/	/
MTRasym (3.5 ppm) (%)]	0.516 (0.286–0.742)	0.909	/	/	/
Grades high (G1+G2) vs low (G3)					
K_{app}	0.895 (0.807–0.952)	< 0.001	0.880	92.31% (75/81)	80.88% (66/81)
D_{app} ($\times 10^{-3}$ mm^2/s)	0.781 (0.675–0.865)	< 0.001	1.033	69.23% (56/81)	83.82% (68/81)
APTWI [MTRasym (3.5 ppm) (%)]	0.749 (0.641–0.839)	< 0.001	3.650	61.54% (50/81)	82.35% (67/81)
DKI (K_{app}+D_{app})	0.906 (0.821–0.960)	< 0.001	/	/	/

AUC (type I vs type II): DKI > APTWI ($Z = 2.042$, $p = 0.041$); AUC (High vs Low): K_{app} > MTRasym (3.5 ppm) ($Z = 2.031$, $p = 0.042$), DKI > APTWI ($Z = 2.013$, $p = 0.044$). The AUC of other parameters between different groups was not significant

EC and high- and low-grade EA, while in the identification of EA and non-EA, only the difference in K_{app} was significant, which was consistent with previous studies [19, 23]. In addition, we have also applied multivariable analysis to the identification of high- and low-grade EA and the identification of type I and type II EC and found that among many factors, such as age, tumor size, FIGO stage, and DKI- and APTWI-related parameters, only K_{app} was an independent predictor for the histological grade of EA and the clinical type of EC. These results indicate that compared with APTWI, DKI has, to a certain extent, a higher sensitivity in reflecting the histological information of EC. The possible reasons are as follows: (1) differences in mobile protein and polypeptide contents between the different EC groups are less significant than the differences in the diffusion of water molecules; (2) compared with DKI, which is almost only affected by the diffusion state of water molecules, the SI of APTWI is affected not only by the mobile protein and polypeptide contents but also by various factors such as the nuclear Overhauser effect, pH value, fat, and water content [38–40]. Furthermore, it may be difficult for the existing body imaging protocol of APTWI to accurately reflect the SI changes caused by the abovementioned reasons. In clinical practice, compared with APTWI, DKI not only has a relatively short scanning time, but also generates

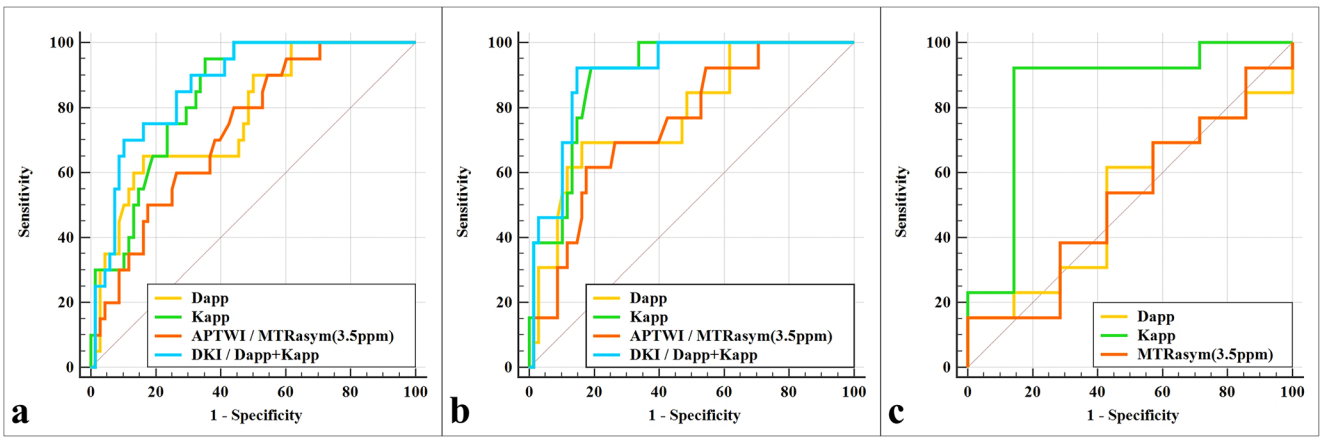

Fig. 4 Graph shows ROC curves to assess utility of different metrics for discriminating different groups. **a** Differentiation of type I from type II EC: different parameters, AUC (K_{app}) > AUC (D_{app}) > AUC (MTRasym (3.5 ppm)), but the difference between AUC of each parameter was not significant ($p > 0.05$); different imaging methods, the AUC (DKI) was nearly significantly higher than AUC (APTWI) ($Z = 2.042$, $p = 0.041$). **b** Differentiation of high- and low-grade EA: different parameters, AUC (K_{app}) > AUC (D_{app}) > AUC (MTRasym (3.5 ppm)), and the difference in AUC between K_{app} and MTRasym (3.5 ppm) values was significant ($Z = 2.031$, $p = 0.042$); different imaging methods, the AUC (DKI) was nearly significantly higher than AUC (APTWI) ($Z = 2.013$, $p = 0.044$). **c** Differentiation of EA and non-EA groups, only the AUC of the K_{app} was significant (AUC = 0.846, $p = 0.003$)

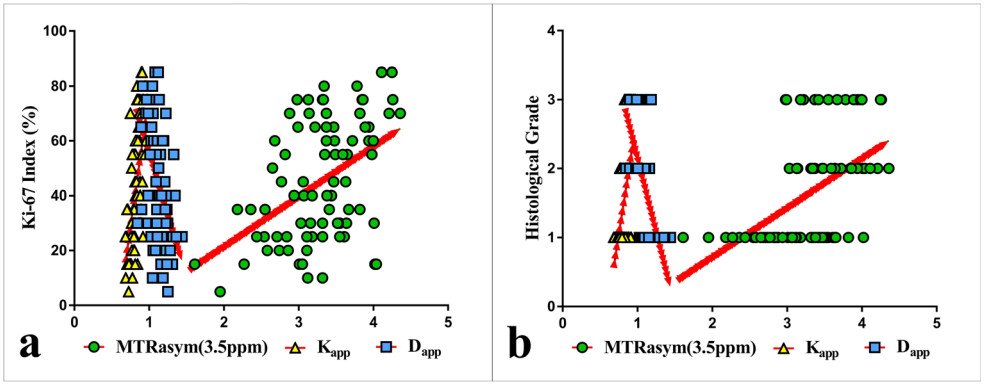

Fig. 5 **a** The Pearson correlation between the Ki-67 index and K_{app}, D_{app}, and MTRasym (3.5 ppm), $r = 0.759$, −0.704, and 0.555, p all < 0.05. **b** The Spearman correlation between histological grade and K_{app}, D_{app}, and MTRasym (3.5 ppm), $r = 0.624$, −0.507, and 0.462, p all < 0.05

DWI images with different *b*-values, which can provide a more sufficient basis for the diagnosis of lesions.

Several limitations of this study need to be pointed out. First, the cohort of this study was relatively small, and it was a single-center study, so there may be selection bias. Second, both APTWI and DKI, based on EPI acquisition, are highly sensitive to motion and susceptibility artifacts, with poor SNR and low spatial resolution, making it difficult to evaluate small EC lesions. Third, we defined the solid portion of EC in the axial plane as the ROIs and used the average value of all slices as the final result, which might hurt histologic heterogeneity. Fourth, in this study, the final value of each lesion parameter is the average of the corresponding parameters on all slices, but due to the heterogeneity of the tumor, this value may not completely match the histological location of the tumor. In the future, we will attempt to adopt the new technology and conduct multicenter prospective cohort and external validation to ensure that this method can be used in clinical practice.

Conclusion

Both DKI- and APTWI-related parameters have potential as imaging markers in estimating the histological features of EC, while DKI shows better performance than APTWI in this study.

Acknowledgements We acknowledge the support received from the National Natural Science Foundation of China and Henan Medical Science and Technology Research Program. In addition, Nan Meng wants to say to Jing Sun: It is graceful grief and sweet sadness to think of you, but in my heart, there is a kind of soft warmth that can't be expressed with any choice of words.

Funding This study has received funding by the National Key R&D Program of China (2017YFE0103600), the Henan Medical Science and Technology Research Program (2018020357 and 2018020367), the National Natural Science Foundation of China (81720108021 and 31470047), the Zhongyuan Thousand Talents Plan Project-Basic Research Leader Talent (ZYQR201810117), and the Zhengzhou Collaborative Innovation Major Project (20XTZX05015).

Declarations

Guarantor The scientific guarantor of this publication is Meiyun Wang.

Conflict of interest One of the authors of this manuscript (Kaiyu Wang) is an employee of GE Healthcare. The remaining authors declare no relationships with any companies whose products or services may be related to the subject matter of the article.

Statistics and biometry No complex statistical methods were necessary for this paper.

Informed consent Written informed consent was obtained from all subjects (patients) in this study.

Ethical approval Institutional Review Board approval was obtained.

Study subjects or cohorts overlap Some study subjects or cohorts have been previously reported in radiology.

Methodology
- prospective
- case-control study
- performed at one institution

References

1. Chen W, Zheng R, Baade PD et al (2016) Cancer statistics in China, 2015. CA Cancer J Clin 66:115–132
2. Fontham E, Wolf A, Church TR et al (2020) Cervical cancer screening for individuals at average risk: 2020 guideline update from the American Cancer Society. CA Cancer J Clin 70:321–346.
3. Bokhman JV (1983) Two pathogenetic types of endometrial carcinoma. Gynecol Oncol 15:10–17
4. Scholten AN, Creutzberg CL, Noordijk EM, Smit VT (2002) Long-term outcome in endometrial carcinoma favors a two- instead of a three-tiered grading system. Int J Radiat Oncol Biol Phys 52:1067–1074
5. Kitson S, Sivalingam VN, Bolton J et al (2017) Ki-67 in endometrial cancer: scoring optimization and prognostic relevance for window studies. Mod Pathol 30:459–468

6. Werner HM, Trovik J, Marcickiewicz J et al (2013) A discordant histological risk classification in preoperative and operative biopsy in endometrial cancer is reflected in metastatic risk and prognosis. Eur J Cancer 49:625–632
7. Garcia TS, Appel M, Rivero R et al (2017) Agreement between preoperative endometrial sampling and surgical specimen findings in endometrial carcinoma. Int J Gynecol Cancer 27:473–478
8. Nougaret S, Horta M, Sala E et al (2019) Endometrial cancer MRI staging: Updated Guidelines of the European Society of Urogenital Radiology. Eur Radiol 29:792–805
9. Ahmed M, Al-Khafaji JF, Class CA et al (2018) Can MRI help assess aggressiveness of endometrial cancer. Clin Radiol 73: 833.e11–833.e18
10. Bhosale P, Ma J, Iyer R et al (2016) Feasibility of a reduced field-of-view diffusion-weighted (rFOV) sequence in assessment of myometrial invasion in patients with clinical FIGO stage I endometrial cancer. J Magn Reson Imaging 43:316–324
11. Andreano A, Rechichi G, Rebora P, Sironi S, Valsecchi MG, Galimberti S (2014) MR diffusion imaging for preoperative staging of myometrial invasion in patients with endometrial cancer: a systematic review and meta-analysis. Eur Radiol 24:1327–1338
12. Beddy P, Moyle P, Kataoka M et al (2012) Evaluation of depth of myometrial invasion and overall staging in endometrial cancer: comparison of diffusion-weighted and dynamic contrast-enhanced MR imaging. Radiology 262:530–537
13. Inoue C, Fujii S, Kaneda S et al (2015) Correlation of apparent diffusion coefficient value with prognostic parameters of endometrioid carcinoma. J Magn Reson Imaging 41:213–219
14. Jensen JH, Helpern JA, Ramani A, Lu H, Kaczynski K (2005) Diffusional kurtosis imaging: the quantification of non-Gaussian water diffusion by means of magnetic resonance imaging. Magn Reson Med 53:1432–1440
15. Jensen JH, Helpern JA (2010) MRI quantification of non-Gaussian water diffusion by kurtosis analysis. NMR Biomed 23:698–710
16. Qi XX, Shi DF, Ren SX et al (2018) Histogram analysis of diffusion kurtosis imaging derived maps may distinguish between low and high grade gliomas before surgery. Eur Radiol 28:1748–1755
17. Yin J, Sun H, Wang Z, Ni H, Shen W, Sun PZ (2018) Diffusion kurtosis imaging of acute infarction: comparison with routine diffusion and follow-up MR imaging. Radiology 287:651–657
18. Sun K, Chen X, Chai W et al (2015) Breast cancer: diffusion kurtosis MR imaging-diagnostic accuracy and correlation with clinical-pathologic factors. Radiology 277:46–55
19. Meng N, Wang X, Sun J et al (2020) Application of the amide proton transfer-weighted imaging and diffusion kurtosis imaging in the study of cervical cancer. Eur Radiol 30:5758–5767
20. Zhou J, Payen JF, Wilson DA, Traystman RJ, van Zijl PC (2003) Using the amide proton signals of intracellular proteins and peptides to detect pH effects in MRI. Nat Med 9:1085–1090
21. Ohno Y, Yui M, Koyama H et al (2016) Chemical exchange saturation transfer MR imaging: preliminary results for differentiation of malignant and benign thoracic lesions. Radiology 279:578–589
22. Krikken E, Khlebnikov V, Zaiss M et al (2018) Amide chemical exchange saturation transfer at 7 T: a possible biomarker for detecting early response to neoadjuvant chemotherapy in breast cancer patients. Breast Cancer Res 20:51
23. Takayama Y, Nishie A, Togao O et al (2018) Amide proton transfer MR imaging of endometrioid endometrial adenocarcinoma: association with histologic grade. Radiology 286:909–917
24. Yamada I, Sakamoto J, Kobayashi D et al (2019) Diffusion kurtosis imaging of endometrial carcinoma: correlation with histopathological findings. Magn Reson Imaging 57:337–346
25. Jia G, Abaza R, Williams JD et al (2011) Amide proton transfer MR imaging of prostate cancer: a preliminary study. J Magn Reson Imaging 33:647–654
26. Mitra AP, Birkhahn M, Cote RJ (2009) Re: Joseph Chin. In Search of the Perfect Crystal Ball for Ta Urothelial Cancer. Eur Urol. 10.1016/j.eururo.2009.09.014. Eur Urol 57:23–24
27. Voss MA, Ganesan R, Ludeman L et al (2012) Should grade 3 endometrioid endometrial carcinoma be considered a type 2 cancer-a clinical and pathological evaluation. Gynecol Oncol 124: 15–20
28. Togao O, Yoshiura T, Keupp J et al (2014) Amide proton transfer imaging of adult diffuse gliomas: correlation with histopathological grades. Neuro Oncol 16:441–448
29. Zheng S, van der Bom IM, Zu Z, Lin G, Zhao Y, Gounis MJ (2014) Chemical exchange saturation transfer effect in blood. Magn Reson Med 71:1082–1092
30. Zaino RJ, Kurman RJ, Diana KL, Morrow CP (1995) The utility of the revised International Federation of Gynecology and Obstetrics histologic grading of endometrial adenocarcinoma using a defined nuclear grading system. A Gynecologic Oncology Group study. Cancer 75:81–86
31. Dobrzycka B, Mackowiak-Matejczyk B, Kinalski M, Terlikowski SJ (2013) Pretreatment serum levels of bFGF and VEGF and its clinical significance in endometrial carcinoma. Gynecol Oncol 128: 454–460
32. Fukunaga T, Fujii S, Inoue C et al (2015) Accuracy of semiquantitative dynamic contrast-enhanced MRI for differentiating type II from type I endometrial carcinoma. J Magn Reson Imaging 41: 1662–1668
33. Li B, Sun H, Zhang S, Wang X, Guo Q (2019) The utility of APT and IVIM in the diagnosis and differentiation of squamous cell carcinoma of the cervix: a pilot study. Magn Reson Imaging 63: 105–113
34. Zhao X, Wen Z, Zhang G et al (2013) Three-dimensional turbo-spin-echo amide proton transfer MR imaging at 3-Tesla and its application to high-grade human brain tumors. Mol Imaging Biol 15:114–122
35. Heo HY, Zhang Y, Lee DH et al (2017) Accelerating chemical exchange saturation transfer (CEST) MRI by combining compressed sensing and sensitivity encoding techniques. Magn Reson Med 77:779–786
36. Rutgers JK (2015) Update on pathology, staging and molecular pathology of endometrial (uterine corpus) adenocarcinoma. Future Oncol 11:3207–3218
37. Xiao Z, Zhong Y, Tang Z et al (2018) Standard diffusion-weighted, diffusion kurtosis and intravoxel incoherent motion MR imaging of sinonasal malignancies: correlations with Ki-67 proliferation status. Eur Radiol 28:2923–2933
38. Khlebnikov V, Polders D, Hendrikse J et al (2017) Amide proton transfer (APT) imaging of brain tumors at 7 T: The role of tissue water T1 -Relaxation properties. Magn Reson Med 77:1525–1532
39. Zhang S, Keupp J, Wang X et al (2018) Z-spectrum appearance and interpretation in the presence of fat: Influence of acquisition parameters. Magn Reson Med 79:2731–2737
40. Liu R, Zhang H, Niu W et al (2020) Erratum to: improved chemical exchange saturation transfer imaging with real-time frequency drift correction (Magn Reson Med. 2019; 81: 2915-2923). Magn Reson Med 83:1884